



A Mathematical Model Of Blood Flow Of A Stenosed Artery In Variable Shape

Goutam Das^{1*}, Bhawna Agrawal², Sanjit Kumar³

^{1*2}Department of Mathematics, Rabindranath Tagore University, Bhopal (M.P), India,

¹Email: mailmeatgoutam@gmail.com, ²Email: bhawnakhushiagrawal@gmail.com

³Department of Mathematics, Lakshmi Narain College of Technology & Science, Bhopal (M.P), India,
Email: sanjeetkumarmath@gmail.com

***Corresponding Author:** Goutam Das

**Department of Mathematics, Rabindranath Tagore University, Bhopal (M.P), India,
Email: mailmeatgoutam@gmail.com*

Article History	Abstract
<p>Received: Revised: Accepted:</p> <p>CC License CC-BY-NC-SA 4.0</p>	<p>In this theoretical study, a mathematical model is developed to carry out a systematic analysis of flow behaviour in a two-dimensional vessel (modeled as artery) with a locally variable shaped constriction. An artificial artery, which containing a viscous incompressible fluid that representing the flowing blood can be treated as inflexible vessel. The shape of the stenosis in the arterial lumen is chosen to be symmetric as well as asymmetric about the middle cross section is perpendicular to the axis of the vessel. The constricted vessel is resolved into a straight vessel and the entire resulting equations are solved by a numerical method with Reynolds number and 'n', a number giving the shape of the constriction as parameters. The impacts of these parameters on wall shear stress, pressure gradient and velocity have been analysed. It is found that the flow resistance decreases as the shape of a smooth stenosis changes and extreme resistance is attained for the symmetric stenosis. But the length of separation increases for the asymmetric constrictions and the oscillation in the shear layer appears earlier for asymmetric constriction than that in the case of symmetric constriction. The extreme resistance is attained for inflexible stenosed vessel rather than the flexible one.</p> <p>Keywords: <i>Two-dimensional vessel, Artificial artery, Incompressible, Stenosed artery, Reynolds number, Resistance, asymmetric.</i></p>

INTRODUCTION:

Blood is a specialized fluid containing a suspension of magnetic particles, specifically red blood cells, within non-magnetic plasma due to the presence of haemoglobin (an iron-based compound) in these cells. Stenosis refers to the narrowing of the inner surface of arteries or openings and it can lead to various circulatory issues by restricting or completely blocking blood flow. When blood flow is compromised in arteries supplying the brain, it can result in cerebral strokes while in coronary arteries, it can lead to myocardial infarction and subsequently, heart failure. The exact causes of stenosis are not fully understood but it has been suggested that cholesterol buildup in arterial walls and the proliferation of connective tissues may contribute to this

condition. Vascular fluid dynamics are reported to play a crucial role in the development and progression of these pathological conditions.

Atherosclerosis is made by cholesterol, fats and other elements in and on the artery walls. It is also called plaque. The plaque can be caused by narrow arteries and blocking of blood flow. The plaque can explode, leading to a blood clot. Although atherosclerosis is mostly considered as a serious problem in the heart, but it can also affect arteries in the whole body. Atherosclerosis can be treated. The prevention of atherosclerosis is possible by the habits of a healthy lifestyle. Atherosclerosis is a disease which severely influences human health. It is characterized by the hardening and thickening of the arterial walls due to the formation of plaque. The formation of plaque minimises the arterial passage area creating uncharacteristic blood flow patterns with the advanced level of disease. As a result, it can cause individuals to suffer cardiac arrest or stroke. Stenoses have a complex influence on haemodynamics through and beyond the narrowed arterial segment. Atherosclerotic disease tends to be localized in the regions of geometrical obliquity such as branch of vessel, curved and stenotic sites and tapered arteries. Coronary artery disease which is the largest single cause of mortality in developed nations occurs when the coronary arteries narrow to such an extent that they are unable to carry out sufficient blood to the heart muscle for it to function efficiently. There are two important causes of death from disease of coronary artery are rupture of the plaque to make sudden occlusion of the artery and the slow increase of a stenosis in the artery due to atherosclerosis. The increase of stenosis can reduce blood flow and also causes debilitation.

Atherosclerosis is the result of the accumulation of cholesterol, fats and other substances within the walls of arteries, forming what is commonly referred to as plaque. This plaque can lead to the narrowing of arteries and blockages, potentially causing them to rupture and form blood clots. While atherosclerosis is often associated with heart-related issues, it can impact arteries throughout the body. Fortunately, atherosclerosis is a treatable condition and its prevention is achievable through adopting a healthy lifestyle.

Atherosclerosis is a severe ailment that significantly impacts human health. It is characterized by the hardening and thickening of arterial walls due to plaque formation. This narrowing of the arterial passage leads to abnormal blood flow patterns as the disease progresses. Consequently, it can result in heart attacks or strokes for affected individuals. Stenosis, a narrowing of arteries, has a complex impact on blood flow both within and beyond the constricted segment of the artery.

Atherosclerotic disease tends to develop in regions where arteries have unusual shapes, such as branching points, curved sections, and narrowed areas. Coronary artery disease, the leading cause of mortality in developed countries, occurs when the coronary arteries narrow to the point where they cannot supply sufficient blood to the heart muscle for it to function effectively. Two key factors contributing to fatal coronary artery disease are the sudden blockage of an artery due to plaque rupture and the gradual increase in arterial narrowing as a result of atherosclerosis. This increasing stenosis not only reduces blood flow but also results in debilitation.

To gain a comprehensive understanding of stenosis development from a physiological perspective, one must possess a deep knowledge of how blood flows within the body and be well-versed in the mechanical properties of the vascular wall under normal physiological conditions. Having the ability to describe how blood flows through a stenosed artery offers the potential for early disease diagnosis, sometimes even before the stenosis becomes clinically significant, and forms the foundation for surgical interventions. Timely interventions by cardiologists significantly reduce the risk of fatal outcomes. Mathematical modeling plays a crucial role in predicting blood flow patterns in arteries affected by atherosclerosis. It enhances the understanding and expertise of cardiologists and contributes to insights into the origin and progression of stenosis development. This technique enables the prediction of hemodynamic characteristics, including pressure, shear stress, velocity and reductions in blood flow.

In recent years, there has been a significant increase in both experimental and theoretical research efforts, exploring different aspects of arterial biomechanics concerning blood flow in arteries with varying shapes that have developed stenosis. Following Young's pioneering numerical investigation into the hemodynamic features of a stenosed artery in 1970, several researchers (including Forrester and Young in 1970, Morgan and Young in 1974, Lee and Fung in 1970, Johnson and Kilpatrick in 1990) have delved into the hemodynamics of stenosed arteries. They did so by modeling the geometric shape of the stenotic lumen with a smooth curve like a cosine. However, it's crucial to emphasize that the interior of a stenosed artery isn't

characterized by smoothness; rather, it features an intricate landscape of numerous small valleys and ridges. Young (1968) conducted research to explore the blood flow through an arterial stenosis and to observe the flow patterns within stenosed arteries. Additionally, Lee and Fung (1970) delved into numerical results concerning the distribution and flow patterns of parameters such as velocity, pressure and shear stress at various Reynolds numbers in the context of blood flow through locally constricted arteries. These blood flow models typically involve a single-layered approach. Kumar et.al. (2014) have analytically studied on blood flow through various stenosis shapes and the slip velocity at the arterial wall in the context of mild stenosis. Within this analytical investigation, they briefly addressed the geometry of the interface between the peripheral layer and the core region, offering numerical insights. In a separate study by Kankane and Bodke (2017), the focus was on the radial velocity of blood in stenosed arteries and the associated shape function. Their findings indicated that the radial velocity profile exhibited negative values as time increased from 0.3 s to 0.5 s, leading to the occurrence of backflow.

A mathematical model and numerical simulation of blood flow through tapered artery was introduced by Shah et. al. (2016). Their findings indicated that as the extremity is approached, wall shear stress increases but it decreases for varying tapering angles. Sahu et.al (2010) conducted a study for examining the arterial blood flow in stenosed vessel using non-Newtonian couple stress fluid model. Basu et.al (2012) investigated a mathematical model based on a non-Newtonian two-phase fluid for blood flow through stenosed arteries. But again Basu et.al (2013) proposed a non-Newtonian fluid model for blood flow using the power law model through an arterial segment affected by atherosclerosis, considering velocity at the wall. In all of these models, the thickness of the peripheral layer is assumed in advance. It would be of significant interest to derive an analytical expression for the peripheral layer depth in terms of measurable flow variables such as flow rates, pressure gradients and more. Kumar et.al (2020) gave an idea on comparative study of non-Newtonian physiological blood flow through elastic stenotic artery with rigid body stenotic artery. Again Kumar et.al (2022) worked on a two-layered model of blood flow for stenosed artery along with the peripheral layer. Rakshit et.al (2023) worked on a mathematical model of flow of blood in a segment of an artery by a non-homogeneous approach.

While considerable research has been conducted in recent decades to explore blood flow in stenosed arteries, there has been a limited focus on understanding blood flow across arteries with varying shapes and sizes of stenosis. Thus the present work was motivated to investigate the blood flow of a stenosed artery in variable shape in the various percentage of area of stenosis.

Equations of Motion: Consider an axi-symmetric and laminar separated flow within a constricted tube, the constriction occurring at a designated location; it is possible to simulate the blood flow through an axi-symmetric stenosis using a two-dimensional approach by employing a cylindrical coordinate system.

Let us consider the cylindrical polar coordinates denoted as (r, θ, z) , with z -axis aligned along the tube's axis of symmetry. The region of interest is $0 \leq r \leq r_0(z)$, $0 \leq z \leq L$, where L represents the finite length of the tube. The in-compressible two-dimensional Navier-Stokes equations can be taken for the modeling of Newtonian blood flow past multiple constrictions. Consider u and v as the components of velocity in the axial and radial directions respectively, p represents fluid pressure, ρ stands for the constant density and ν signifies the kinematic viscosity of the fluid. Let U represent the maximum in flow velocity specified in

the inlet section or test section of the tube. Introducing the non-dimensional variables: $t = \frac{t'U}{D_0}$, $r = \frac{r'}{D_0}$,

$$z = \frac{z'}{D_0}, r_0(z) = \frac{r_0'(z)}{D_0}, u = \frac{u'}{U}, v = \frac{v'}{U}, p = \frac{p'}{\rho U^2},$$

where D_0 is the diameter of the tube in the unobstructed segment.

The fundamental equations governing the in-compressible fluid flow, which address the conservation of mass and momentum fluxes, can be expressed using non-dimensional variables as follows: $r \frac{\partial u}{\partial z} + \frac{\partial vr}{\partial r} = 0$

$$(1)$$

$$\frac{\partial u}{\partial t} + \frac{\partial uv}{\partial r} + \frac{\partial u^2}{\partial z} + \frac{uv}{r} = -\frac{\partial p}{\partial z} + \frac{1}{R_e} \left[\frac{\partial^2 u}{\partial r^2} + \frac{1}{r} \frac{\partial u}{\partial r} + \frac{\partial^2 u}{\partial z^2} \right] \tag{2}$$

$$\frac{\partial v}{\partial t} + \frac{\partial uv}{\partial z} + \frac{\partial v^2}{\partial r} + \frac{v^2}{r} = -\frac{\partial p}{\partial r} + \frac{1}{R_e} \left[\frac{\partial^2 v}{\partial r^2} + \frac{1}{r} \frac{\partial v}{\partial r} + \frac{\partial^2 v}{\partial z^2} - \frac{v}{r^2} \right] \tag{3}$$

where $R_e = \frac{uD_0}{\nu}$ is the Reynolds number.

Boundary Conditions: Along the axis of symmetry, the normal component of velocity and shear stress diminishes so that $\frac{\partial u(z, r, t)}{\partial r} = 0, v(z, r, t) = 0$ on $r = 0$

$$(4)$$

The velocity boundary conditions at the arterial wall, when considered as rigid, adhere to the standard no-slip conditions, which are expressed as:

$$u(z, r, t) = v(z, r, t) = 0 \text{ at } r = r_0(z) \tag{5a}$$

While those in the case of flexible wall are:

$$u(z, r, t) = 0, v(z, r, t) = \frac{\partial r_0(z, t)}{\partial t} \text{ on } r = r_0(z, t) \tag{5b}$$

In the governing equations of the model, it was assumed that the flow regime is laminar. Furthermore, the model assumed that the flow is fully developed at the inlet test section of the tube, with the inlet section positioned at $z = 0$. The inlet velocity conditions are considered to have a parabolic profile, which corresponds to Hagen-Poiseuille flow through an elongated circular tube as: $u(z, r, t) = 2(1 - r^2)$, $v(z, r, t) = 0$ at $r = 0$

$$(6)$$

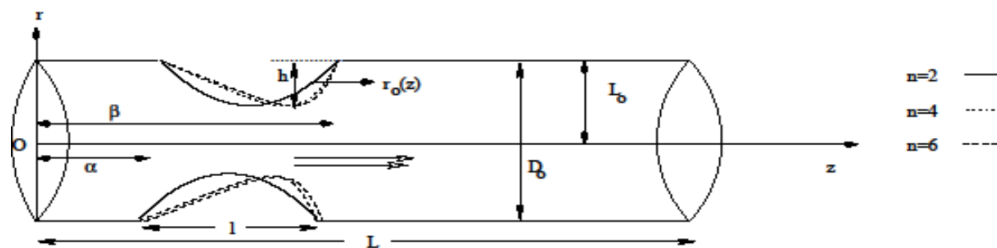


Figure: 1(a) Geometry of the tube with symmetric as well as asymmetric constrictions.

In Figure. 1(a), the downstream length (β) is long enough to ensure that the reattachment length remains unaffected by the size of the calculation domain. The zero velocity gradient boundary conditions are applied

at the outlet cross-section of the tube. $\frac{\partial u(z, r, t)}{\partial z} = 0, \frac{\partial v(z, r, t)}{\partial z} = 0$

$$(7)$$

Initial Condition: The initial condition stipulates that within the specified tube region, there is no flow except for the parabolic velocity profile at the inlet. As time progresses, the flow continuously develops.

Transformation of basic equations: Consider a co-ordinate stretching in the radial direction that converts

the constricted tube into a straight circular tube, as given by: $R = \frac{r}{r_0(z)}, 0 < r < r_0$

$$(8)$$

Where the function $r_0(z)$ is defined as:

$$r_0(z) = \begin{cases} L_0 \left[1 - K_0 \left[l^{n-1} (z - \alpha) - (z - \alpha)^n \right] \right], & \alpha \leq z \leq \beta \\ L_0, & \text{otherwise} \end{cases} \quad (9)$$

In this context, $r_0(z)$ denotes the radius of the tube in the constricted region. The parameters include α , which signifies the distance from the beginning of the segment to the start of the stenosis, β , indicating the distance from the start of the segment to the end of the stenosis, n (where $n \geq 2$) is a parameter influencing the shape of the stenosis, l stands for the length of the stenosis, L_0 represents the unstricted radius of the tube. Here the constant K_0 is given by:

$$K_0 = \frac{h}{L_0} \frac{n^{n-1}}{l^n n - 1}, \quad \text{where } h \text{ is the height of the stenosis.}$$

All the profiles described by equation (9) seem to be static and not time-dependent (rigid) and we can easily incorporate their time-dependent behaviour in such a way that:

$$r_0(z, t) = r_0(z) \cdot a_1(t), \quad \text{where } a_1(t) = 1 + k \cos(\omega t - \varphi) \text{ with the amplitude parameter } k, \text{ the phase angle } \varphi \text{ and the angular frequency } \omega.$$

The analysis in this study focuses on a schematic diagram of a constricted tube geometry with various shapes, as shown in Figure 1(a). The study considers all relevant parameters. For low Reynolds numbers, a finite length of 60 is used to represent the flow. However, for high Reynolds numbers, an appropriate length is chosen to ensure that the reattachment length is not influenced by the downstream distance. In this research, we consider values of n equal to 2, 4 and 6, resulting in symmetric (centered), slightly asymmetric, and severely asymmetric constrictions, each with a width of 14 units.

Numerical computations: The governing equations for viscous, incompressible fluid flows are converted into discrete form using finite-difference approximations. In this study, we employ the widely recognized staggered grid approach introduced by Harlow and Welch in 1965. When discretizing the continuity equation at the (i, j) cell location, we obtain the following:

$$R_j r_0(z_i) \frac{u_{i,j}^n - u_{i-1,j}^n}{\delta z} - R_j^2 \frac{\partial r_0(z_i)}{\partial z} \frac{utc - ubc}{\delta R} + \frac{R l_j v_{i,j}^n - R l_{j-1} v_{i,j-1}^n}{\delta R} = 0 \quad (10)$$

where utc and ubc are defined as follows:

$$utc = 0.25 \left(u_{i,j}^n + u_{i-1,j}^n + u_{i-1,j+1}^n + u_{i,j+1}^n \right),$$

$$ubc = 0.25 \left(u_{i,j}^n + u_{i-1,j}^n + u_{i,j-1}^n + u_{i-1,j-1}^n \right)$$

Taking into account the source, convective and diffusive terms at the n^{th} time step, the finite difference representation of the momentum equation in the z -direction can be formulated as follows:

$$\frac{u_{i,j}^{(n+1)} - u_{i,j}^n}{\delta t} = \frac{p_{i,j}^n - p_{i+1,j}^n}{\delta z} + \frac{R_j}{r_0(z l_i)} \frac{\partial r_0(z l_i)}{\partial z} \frac{pt - pb}{\delta R} + Ucd_{i,j}^n = 0 \quad (11)$$

where the terms pt , pb and $Ucd_{i,j}^n$ are defined as follows:

$$pt = 0.25 \left(p_{i,j}^n + p_{i+1,j}^n + p_{i,j+1}^n + p_{i+1,j+1}^n \right),$$

$$pb = 0.25 \left(p_{i,j}^n + p_{i+1,j}^n + p_{i,j-1}^n + p_{i+1,j-1}^n \right),$$

$$Ucd_{i,j}^n = \frac{1}{R_e} Diff u_{i,j}^n - Conu_{i,j}^n$$

The finite difference equation that provides an approximation for the momentum equation in the R-direction is:

$$\frac{v_{i,j}^{(n+1)} - v_{i,j}^n}{\delta t} = \frac{1}{r_0(z)} \frac{p_{i,j}^n - p_{i,j+1}^n}{\delta R} + Vcd_{i,j}^n \quad (12)$$

$$\text{where: } Vcd_{i,j}^n = \frac{1}{R_e} Diff v_{i,j}^n - Con v_{i,j}^n$$

Here $Vcd_{i,j}^n$ represents the discretization of the convective and diffusive terms in the v -momentum equation at time step n for the cell (i, j) . The treatment of the diffusive and convective terms in the v -momentum equations is analogous to the approach used for the u -momentum equations, particularly with regard to the convective flux. The Poisson equation governing pressure is derived by combining the discretized versions of both the momentum and continuity equations. The resulting expression for the final form of the Poisson equation for pressure is:

$$\begin{aligned} & (A + B + C + D) p_{i,j}^n - A p_{i+1,j}^n - B p_{i-1,j}^n + A_1 p_{i+1,j+1}^n - A_1 p_{i+1,j-1}^n - A_2 p_{i-1,j+1}^n + A_2 p_{i-1,j-1}^n \\ & - (C - A_1 + A_2) p_{i,j+1}^n - (D + A_1 - A_2) p_{i,j-1}^n \\ & = - \left[\frac{D_i v_{i,j}^n}{\delta t} + R_j r_0(z_i) \frac{Ucd_{i,j}^n - Ucd_{i-1,j}^n}{\delta z} + \frac{R_l Vcd_{i,j}^n - R_{l-1} Vcd_{i,j-1}^n}{r_0(z l_i)} \right] \end{aligned} \quad (13)$$

The values A, B, C, D, A_1, A_2 are provided in the work by Layek et al. (2005). Here $D_i v_{i,j}^n$ represents the finite difference representation of the velocity field's divergence at the cell (i, j) . Subsequently, the ultimate version of the Poisson equation is solved iteratively while considering suitable boundary conditions. The pressure-velocity correction formulas are applied repeatedly until a desirable level of divergence is attained.

Stability criteria of the scheme: The time step (δt) is determined based on two criteria as outlined below. The first criterion ensures that the fluid does not traverse more than a single cell within one time step, adhering to the Courant, Friedrichs and Lewy condition. Hence, the time step must meet the following conditions:

$$\delta t \leq Min \left[\frac{\delta z}{|u|}, \frac{\delta R}{|v|} \right]_{i,j} \quad (14)$$

where minimum is taken in the global sense. Secondly, momentum must not diffuse more than one cell in one time step. This condition, which is related to the viscous effects, implies

$$\delta t \leq Min \left[\frac{R_e}{2} \frac{\delta z^2 \cdot \delta R^2}{(\delta z^2 + \delta R^2)} \right]_{i,j} \quad (15)$$

By representing the right-hand side of equations (14) and (15) as (δt_1) and (δt_2) respectively, we can observe that both of these inequalities are met when the time step (δt) adheres to the following condition:

$$\delta t \leq Min[\delta t_1, \delta t_2] \quad (16)$$

Hence, in our computations we take:

$$\delta t = c \text{Min}[\delta t_1, \delta t_2] \quad (17)$$

Where, c is a constant lying between 0.2 to 0.4. A typical value of (δt) is 0.005 for a $\delta z = 0.005$ and $\delta R = 0.05$.

Results and Discussions:

In this theoretical investigation, we varied the numerical values associated with the specific stenosed artery geometry used for simulations and the parameters required for numerical computations of important physiological quantities. This was done to explore a range of values around typical values, aiming to obtain results that hold physiological significance:

$$\alpha = 10, \beta = 24, l = 14, L_0 = \frac{D_0}{2} = 1, n = 2(4, 6), h = (0.5), k = 0.001,$$

$$\omega = 2\pi \times 1.2 \text{Hz}, \phi = 180.$$

The computed results are obtained by the above mentioned numerical scheme (taking) for various physical quantities of major physiological significance. In order to have their quantitative measures they are all exhibited through the figures 3-11 and discussed at length.

The computed results were generated using the previously described numerical method, with specific parameters (such as $\delta t = 0.005$ for $\delta z = 0.05$ and $\delta R = 0.005$), for a range of crucial physiological variables. To provide quantitative insights, these results are visually presented in figures 3 to 11 and are extensively discussed in detail.

Although the arterial constriction typically follows a smooth curve, it also exhibits numerous smaller variations akin to ridges and valleys, reminiscent of a mountain range. To thoroughly investigate this issue, published data from Back et al. (1984) were utilized to define the shape of the stenosis, as depicted in Figure 1(b). In comparing our findings with those of Back et al. (1984), Johnston and Kilpatrick (1991) and Andersson et al. (2000), we occasionally ignored the arterial wall's dispensability. However, we also paid close attention to cases involving a compliant wall model.

We compared the wall shear stress, as shown in Figure 2(a), with the results obtained in the present investigation using a two-stage numerical approach for the scenario of an asymmetric single constriction with irregular surface geometry (refer to Figure 1(b)). This comparison was carried out for Reynolds numbers $R_e = 20$ and $R_e = 1000$. Notably, our findings closely match those of Johnston and Kilpatrick (1991).

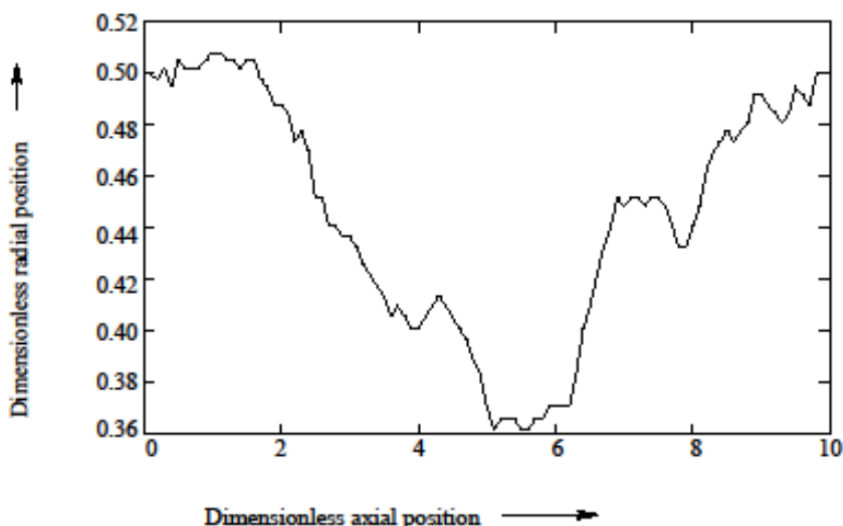


Figure: 1(b) Profile of irregular stenosis (Back et.al. 1984)

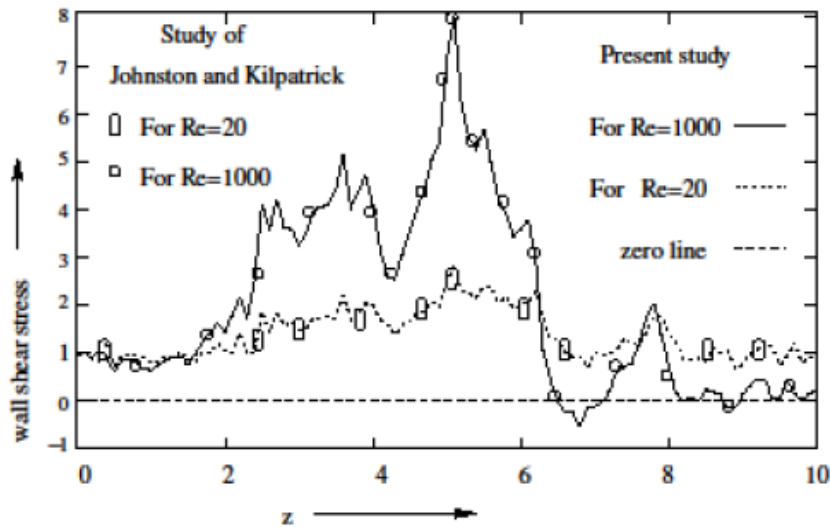


Figure: 2(a) Comparison of wall shear stresses for irregular model at Reynolds numbers $R_e = 20$ and $R_e = 1000$.

The present study includes an examination of pressure drop in the case of asymmetrical stenosis over a range of Reynolds numbers from 10 to 1000. We compared these results with the numerical findings of Andersson et al. (2000) and the experimental data from Back et al. (1984), as depicted in Figure 2(b). The comparison in Figure 2(b) reveals a substantial agreement between our results and the experimental data from Back et al. (1984). However, there is a slight discrepancy with the numerical results of Andersson et al. (2000). This variation may be attributed to the unsteady flow mechanism employed in the present investigation.

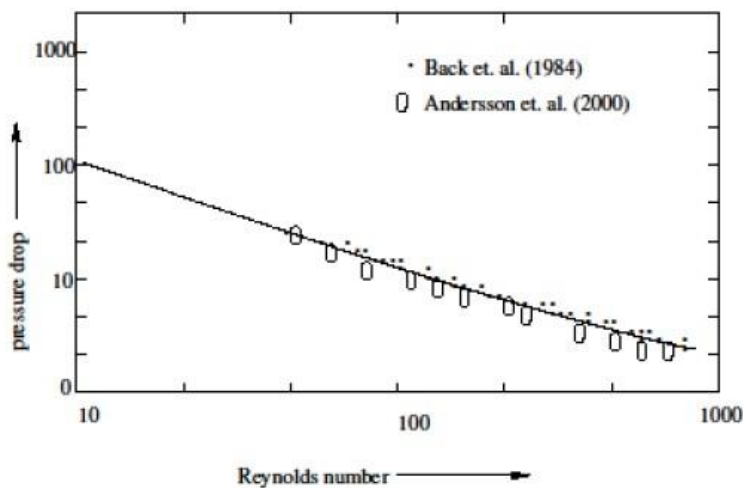


Figure: 2(b) Comparison of non-dimensional pressure drop.

When arteries narrow, such as in the case of a constriction, it results in increased resistance within the flow. Consequently, both shear stress (wall vorticity) and pressure drop also rise, and these parameters are of significant physiological importance.

The distribution of pressure on the arterial wall holds great significance because it plays a key role in the development of post-stenotic dilatation resulting from arterial damage, which is linked to the intricate flow patterns. The variations in pressure on the arterial wall also give rise to fluctuations that generate acoustic signals, which can be detected externally, as discussed by Mittal et al. (2001).

A notable drop in pressure is evident in Fig. 3 as we approach the occlusion, reaching a local minimum that corresponds to the separation point in both symmetric and asymmetric constrictions ($n = 2$ and 4). The two pressure curves exhibit a similar pattern, and when comparing pressure distribution between the two types of stenoses, symmetric and asymmetric, it becomes evident that asymmetric stenosis results in higher pressure

Available online at: <https://jazindia.com>

values, as shown in Fig. 3. Additionally, as the degree of stenosis increases, the reduction in pressure at the constriction's narrowest point decreases significantly, whether it's a symmetric or an asymmetric constriction.

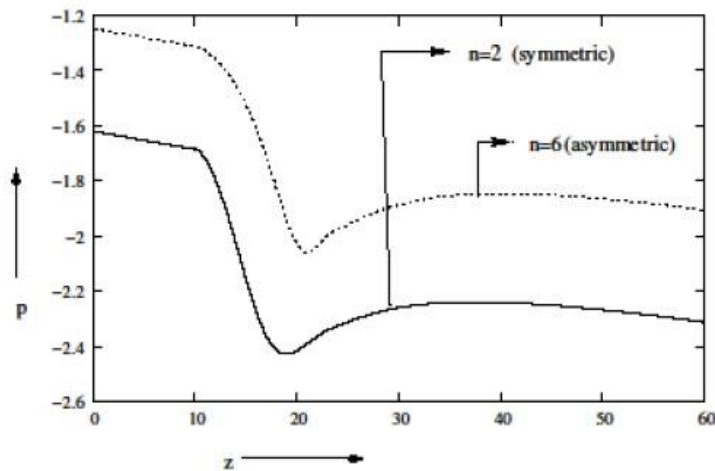


Figure: 3 Pressure distribution along the wall in a tube with symmetric constriction and same in case of asymmetric constriction of same height $h = 0.3$ and $Re = 600$.

Fig. 4 displays the changes in centre line velocity in the axial direction at $Re = 600$ for stenoses of different shapes, with n values of 2, 4 and 6. The figure makes it quite evident that the maximum centre line velocity occurs just slightly downstream of the constriction. This is a result of the recirculation zone formation near the wall due to flow separation. In the case of symmetric constriction ($n = 2$), which is centred, the narrowing in the converging part of the stenosis leads to a more pronounced flow acceleration compared to the asymmetric stenosis ($n = 4$). As the Reynolds number increases, it is observed that the centre line velocity takes a longer distance to return to its initial value.

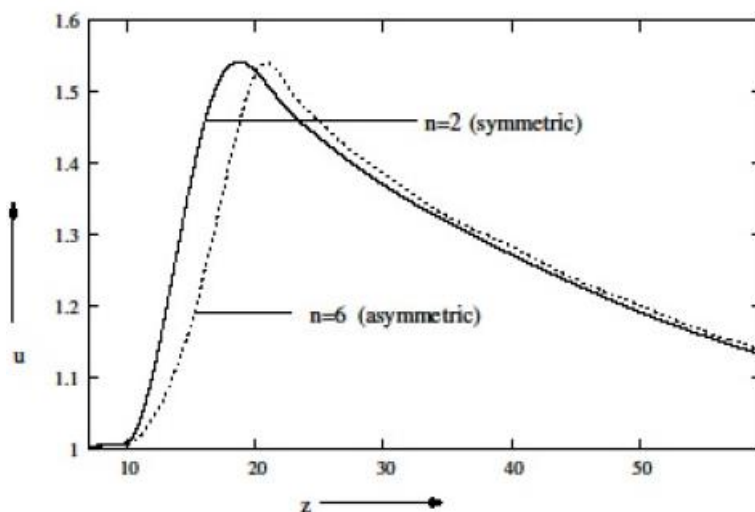


Figure: 4 Centreline u – velocity in a tube with symmetric constriction and same in case of asymmetric constriction of same height $h = 0.3$ and $Re = 600$.

Wall shear stress holds physiological significance, and there are two opposing hypotheses regarding its role in the onset of atherosclerosis. Calculating wall shear stress accurately is a challenging task. In this context, numerical simulations offer valuable insights into the magnitude of wall shear stress. Fig. 5 illustrates the wall shear stress for symmetric ($n = 2$), slightly asymmetric ($n = 4$) and severely asymmetric ($n = 6$) stenoses at a Reynolds number $Re = 220$ with a 51% area reduction ($h = 0.3$). It is evident that in the case of a severely asymmetric constriction ($n = 6$), flow separation occurs, while in the slightly asymmetric constriction ($n = 4$), flow separation initiates. In contrast, there is no flow separation in the case of symmetric constriction ($n = 2$).

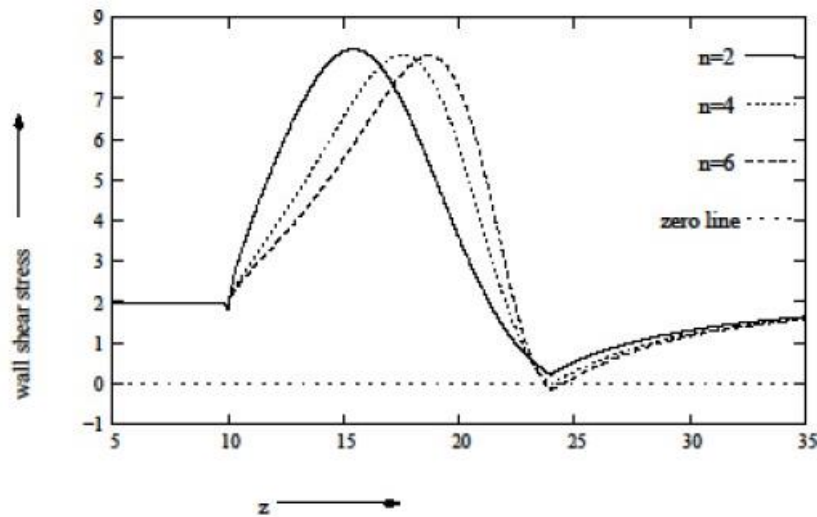


Figure: 5 Wall shear stress distribution in a tube with symmetric constriction and same in case of asymmetric constriction of same height $h = 0.3$ and $R_e = 220$.

In Figure 6, we observe the variation of wall shear stress along both solid and flexible surfaces for differently shaped constrictions at $R_e = 600$ with $h = 0.5$. Notably, the peak vorticity location is right before the plane of minimum constriction for both rigid and flexible wall models. As the flow approaches the constriction, the magnitude of wall shear stress values increases rapidly, reaching a peak value near the point of minimum constriction in all cases. Downstream from this location, the wall shear stress decreases rapidly and turns to negative values when flow separation initiates along the tube wall.

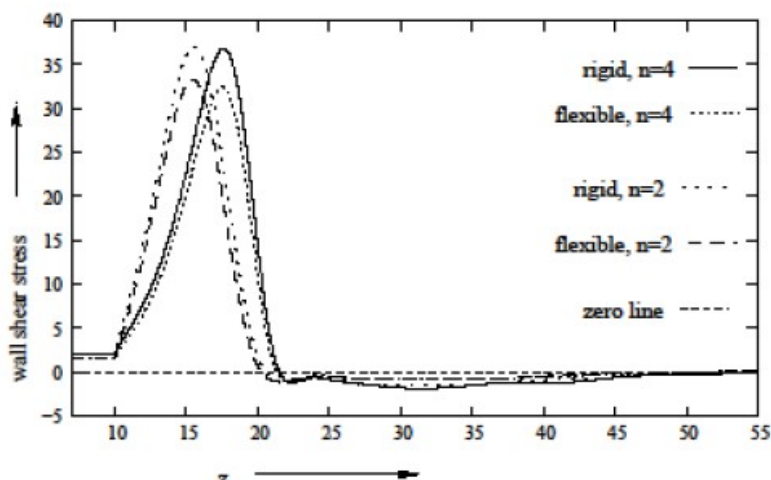


Figure: 6 Wall shear stress distribution in a rigid as well as flexible tube with symmetric constriction and same in case of asymmetric constriction of same height $h = 0.5$ and $R_e = 600$.

The points where vorticity equals zero correspond to stagnation points, as well as the locations where attached vortices separate and reattach. It's also noticeable that the maximum wall shear stress value decreases as the shape of a smooth stenosis becomes more pronounced, with the highest wall shear stress achieved in the case of a symmetric stenosis ($n = 2$). This observation aligns perfectly with the analytical study conducted by Haldar (1985). For both rigid and flexible arteries, a similar trend is observed in the respective wall shear stress distributions, with variations primarily in magnitudes. The highest wall shear stress value is greater in the case of a rigid tube compared to a flexible one. Moreover, in the case of a rigid tube, the point of separation shifts further downstream compared to a flexible tube. In Figure 7, we can observe the influence of stenosis severity on both symmetric and asymmetric cases. In both situations, as the height of the constriction increases, both the peak wall shear stress and the length of the separation zone also increase.

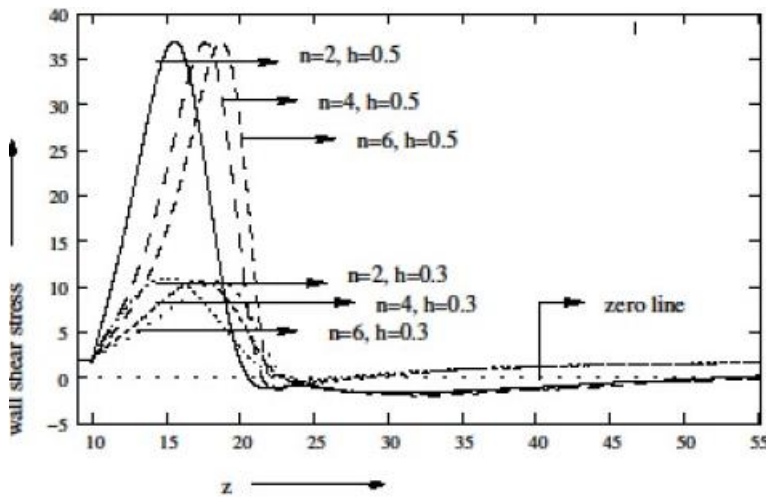


Figure: 7 Comparison of wall shear stress distribution in a tube with symmetric constriction and same in case of asymmetric constriction at $R_e = 600$.

Fig. 8 illustrates the distributions of wall shear stress (τ_w) for Reynolds numbers $Re = 600$ and 1000 . At the highest Reynolds number considered, we observe a similar situation in the converging part of the stenosis, as demonstrated in Fig. 9(a). However, in the downstream diverging part, the deceleration of the fluid is more gradual compared to lower Reynolds numbers, and the axial velocity has not yet reached its asymptotic limit (2) at the downstream end of the stenosis, for both symmetric and asymmetric cases. In the case of asymmetric constrictions, there is an increase in the length of separation, and both the separation point and the reattachment point are shifted further downstream in these scenarios.

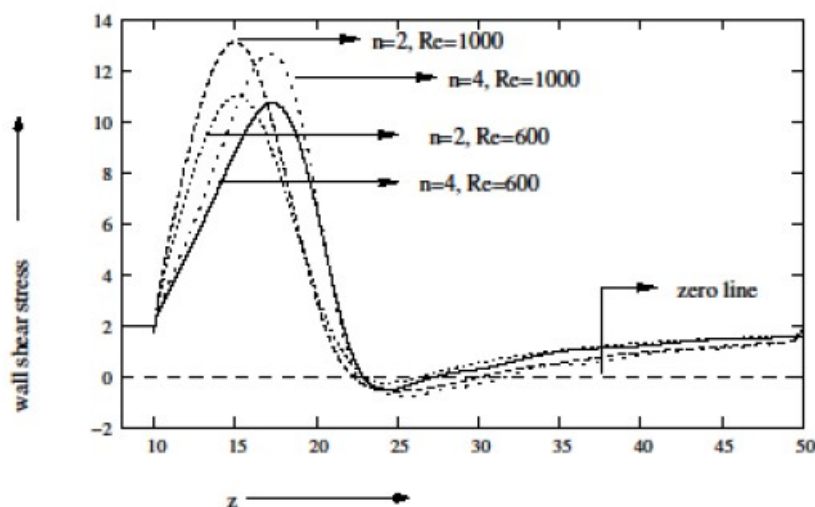


Figure: 8 Comparison of wall shear stress distribution in a tube with symmetric constriction and same in case of asymmetric constriction of same height $h = 0.3$

The level of fluctuation in wall shear stress is of significant interest. It's worth noting that highly variable wall shear stress can increase the susceptibility to atherosclerosis. This variability in shear stress can hinder the alignment of endothelial cells in the direction of flow, potentially making the intima more permeable to the entry of monocytes and lipoproteins. In Fig. 9(a), we observe the oscillatory nature of wall shear stress at $R_e = 1000$ and $h = 0.3$.

It's quite evident from this figure that the oscillations in the shear layer manifest earlier in the case of asymmetric constriction compared to symmetric constriction. Additionally, in asymmetric constrictions, the length of separation increases, and both the separation point and the reattachment point shift further downstream.

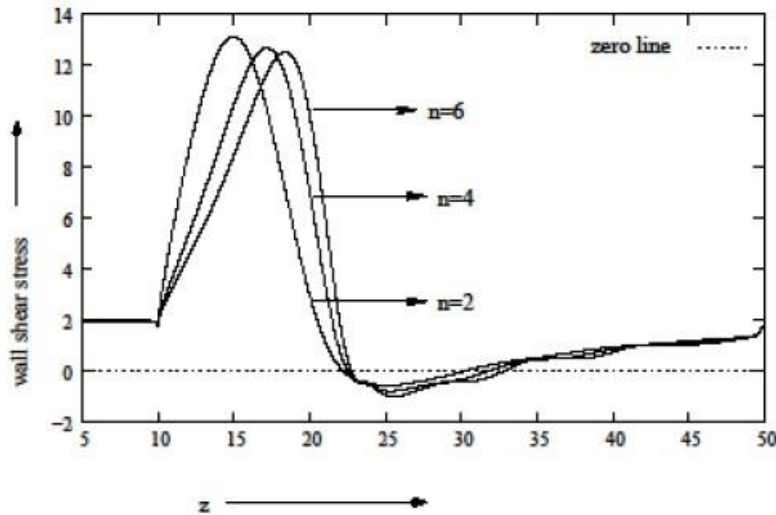


Figure: 9(a) Wall shear stress distribution in a rigid as well as flexible tube with symmetric constriction and same in case of asymmetric constriction of same height $h = 0.3$ and $R_e = 1000$

The dynamic behaviour of blood flow through a distensible artery is highly significant when considering realistic scenarios with stenotic conditions. With this in mind, we examine the time-dependent response of the stream wise velocity component at $R_e = 600$, specifically at $z = 11$ (where z represents the distance from the tube inlet) within the constricted region. This analysis focuses on a 51% area reduction case for asymmetric constriction ($n = 6$) in both rigid and flexible arteries, as depicted in Fig. 9 (b). In both rigid and flexible arteries, we observe substantial distortions in the stream wise velocity component at the initial stage of the simulation. This is followed by a consistently undulating stream wise velocity pattern in the case of the rigid artery. In contrast, the flexible artery exhibits a uniform stream wise velocity for the remainder of the considered time period.

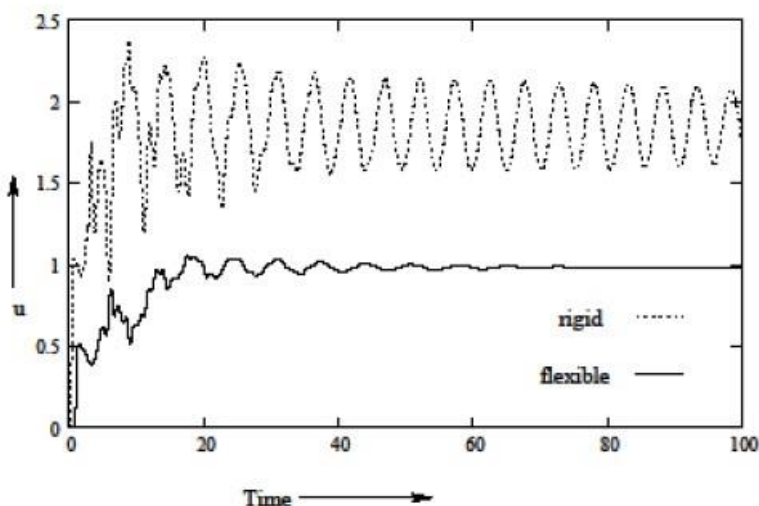


Figure: 9(b) Time history of streamwise velocity component $R_e = 600$ in a rigid as well as flexible tube with asymmetric constriction ($n = 6$) of height $h = 0.3$ at $z = 11$ (in the constricted region)

In Fig. 10(a), we observe oscillations in the stream wise velocity component with a frequency of 0.2 at $z = 11$ (representing the distance from the tube inlet) within the constricted region. This phenomenon occurs at a Reynolds number of 1000 for a 51% area reduction in the case of asymmetric constriction ($n = 6$). It's worth noting that no oscillations are observed upstream of the constriction. Fig. 10(b) presents the time history of the stream wise velocity component at $z = 24$, which is where the constriction ends, under the same

conditions ($Re = 1000$ and 51% blockage for asymmetric constriction, $n = 6$). Here, we observe a different type of oscillation with the same frequency.

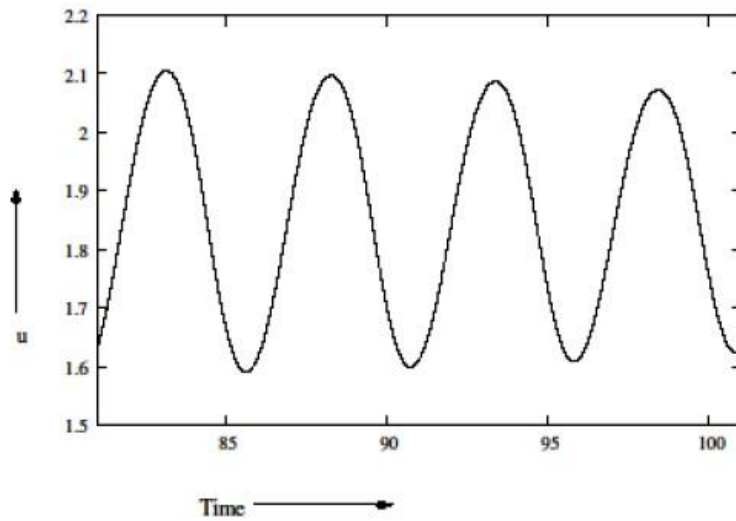


Figure: 10(a) Time history of streamwise velocity component $Re = 1000$ in a rigid as well as flexible tube with asymmetric constriction ($n = 6$) of height $h = 0.3$ at $z = 11$ (in the constricted region)

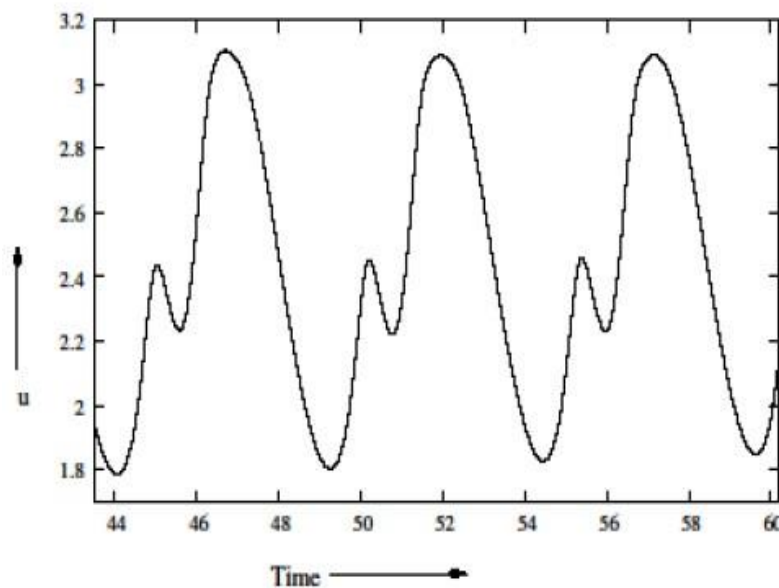


Figure: 10(b) Time history of streamwise velocity component $Re = 1000$ in a rigid as well as flexible tube with asymmetric constriction ($n = 6$) of height $h = 0.3$ at $z = 24$ (in the constricted region)

Figures 11(a), (b), and (c) display the streamline patterns for symmetric ($n = 2$), slightly asymmetric ($n = 4$), and significantly asymmetric ($n = 6$) constrictions, respectively. These figures unmistakably reveal the development of separated regions resembling bubbles downstream of the constriction in each scenario. It's noteworthy that the extent of these circulatory bubble formations increases as the asymmetry of the constriction becomes more pronounced. The degree of constriction asymmetry significantly influences the occurrence of flow separation.

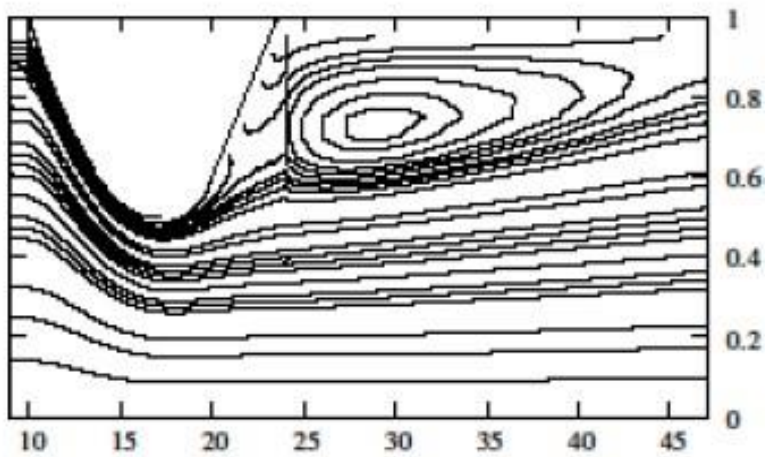


Figure: 11(a) Streamline in a rigid as well as flexible tube with symmetric constriction of 75% area reduction at $R_e = 600$

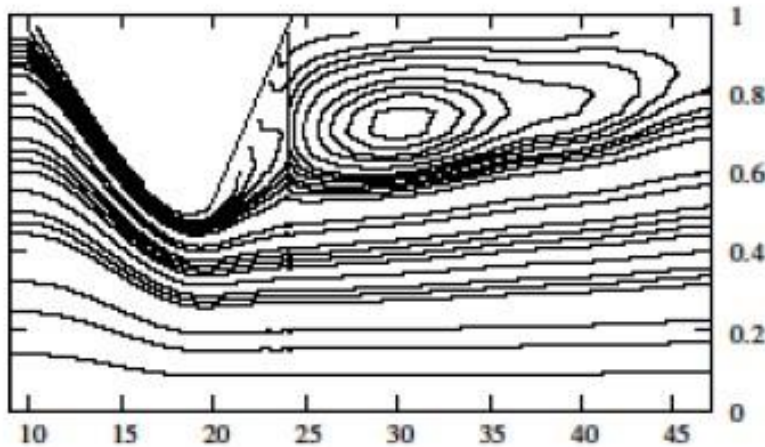


Figure: 11(b) Streamline in a rigid as well as flexible tube with asymmetric constriction ($n = 4$) of 75% area reduction at $R_e = 600$

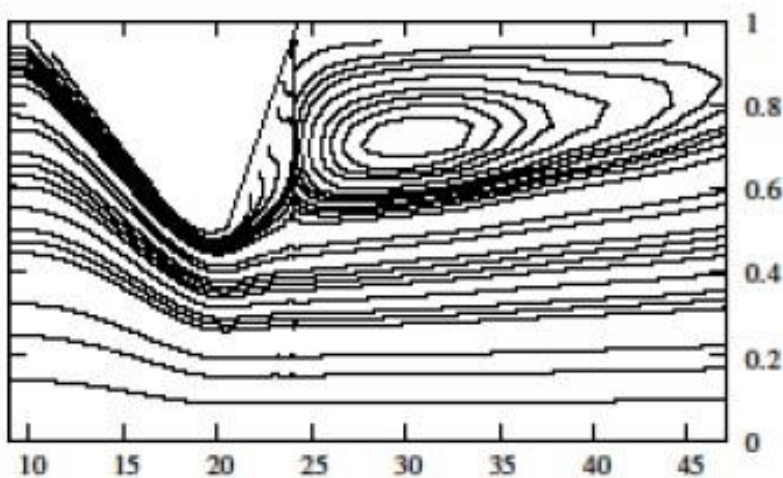


Figure: 11(c) Streamline in a rigid as well as flexible tube with asymmetric constriction ($n = 6$) of 75% area reduction at $R_e = 600$

Conclusion:

This mathematical model addresses blood flow through stenosed arteries of various shapes. A comparison of the results from this current theoretical study with previous ones, which were based on the assumption of Newtonian blood behaviour, rigid arteries and steady-state conditions, demonstrates a notable level of agreement. Consequently, the present model offers a more insightful perspective on the intricate flow phenomena in stenotic situations. This model makes significant progress over previous ones by accounting for unsteadiness and incorporating vessel wall distensibility. It is suggested that the development of a separation region toward the diverging area of the constriction is a key area for the further deposition of atherosclerotic plaques. The presence of an asymmetric constriction in the context of arterial plaque may be beneficial for the early detection of cardiovascular diseases.

REFERENCES:

1. Andersson, H.I., Halden, R. and Glomsaker, T. (2000), Effect of surface irregularities on flow resistance in differently shaped arterial stenoses, *J. Biomech.*, vol. 33(10), pp.1257-1262.
2. Agrawal, B., Kumar, S. and Das, G. (2022), Mathematical model of blood flow through stenosed arteries with the impact of hematocrit on wall shear stress, *International Journal of Applied Research*, vol. 8 (3), pp. 439-443.
3. Agrawal, B., Kumar, S. and Rakshit, S. (2022), A Mathematical study of constrained fluid movement in the arterial system due to the formation of multiple stenosis, *International Journal of Applied Research*, vol. 8 (3), pp. 455-464.
4. Basu Malik, B., Nanda. S. P. (2012), A non- Newtonian two-phase fluid model for blood flow through arteries under stenotic condition, *IJPBS*, vol. 3(3), pp.237-247.
5. Basu Malik, B., Nanda. S. P., Das, B., Saha, D., Das, D.S. and Paul. K. (2013), A non-Newtonian fluid model for blood flow using power law through an atherosclerotic arterial segment having slip velocity, *International Journal of Pharmaceutical, Chemical and Biological Sciences*, vol. 3(3), pp. 752-760.
6. Bugliarello, G. and Sevilla, J. (1970), Velocity distribution and other characteristics of steady and pulsatile blood flow in fine glass tubes, vol.7(2), pp. 85-107.
7. Damno, M. M., Agrawal, B., Kumar, S., Das, G., (2021). A Mathematical model for the blood flow in a modeled artery with a stenosis and an aneurysm. *International Journal of Statistics and Applied Mathematics*, vol. 6(2), pp. 65-71
8. Forrester, J. H. and Young, D. F. (1970), Flow through a converging-diverging tube and its implications in occlusive vascular disease-1: theoretical development, *J. Biomechanics*, vol. 3(1), pp. 297-305.
9. Johnston, P. R. and Kilpatrick, D. (1990), A mathematical model of paired arterial stenoses, *Computers in Cardiology*, pp. 229-232.
10. Johnston, P.R. and Kilpatrick, D. (1991), Mathematical modeling of flow through an irregular arterial stenosis, *J. of Biomech.*, vol. 24(11), pp.1069-1077.
11. Kankane, N.D. and Bodke, N.S. (2017), The study of radial velocity of blood through stenosed artery and shape function, *Palestine Journal of Mathematics*, vol. 6(1), pp. 324-329
12. Kumar, H., Chandel, R.S., Kumar, S. and Kumar, S. (2014), A mathematical model for different shapes of stenosis and slip velocity at the wall through mild stenosis artery, *Advances in Applied Mathematical Biosciences*, vol. 5(1), pp. 9-18.
13. Khan, R. A. and Agrawal, B. D. (2021), Analysis of fluid flow through channels with slip boundary: Mathematical study, *International Journal of Statistics and Applied Mathematics*, vol. 6(1), pp.134-137.
14. Kumar, S., Kumar, S., Kumar, D. (2020), Comparative study of non- Newtonian physiological blood flow through elastic stenotic artery with rigid body stenotic artery, *Series on Biomechanics*, vol. 34 (4): 26-41.
15. Kumar, S., Kumar, S., Kumar, D. and Kumar, A. (2022), A two- layered model of blood flow for stenosed artery along with the peripheral layer, *Series on Biomechanics*, vol. 36 (2): 181-187.
16. Khoja, I. M., and Agrawal, B. (2021), Mathematical modeling of blood flow, *International Journal of Statistics and Applied Mathematics*, vol. 6(4), pp. 116-122.
17. Lee, J. S. and Fung, Y. C. (1970), Flow in locally constricted tubes at low Reynolds numbers, *J. Appl. Mech.*, vol. 37(1), pp. 9-16.

18. Mir, A. M., and Agrawal, B. D. (2021), A Mathematical study of DNA complexes of one-bond edge type. *Journal of Mathematical problems, equations and Statistics*, vol. 2(2) pp. 08-16.
19. Morgan, B. and Young, D. (1974), An integral method for the analysis of flow in arterial stenoses, *Bull. Math. Biol.*, vol. 36(4), pp. 39-53.
20. Mukhopadhyay, S. and Layek, G. C. (2008), Numerical modeling of a stenosed artery using mathematical model of variable shape, *Applications and Applied Mathematics*, vol. 3(6), pp. 308 - 328.
21. Rakshit, S., Agrawal, B. and Kumar, S. (2023), A Mathematical model of flow of blood in a segment of an artery by a non-homogeneous approach", *Journal of Data Acquisition and Processing*, vol. 38 (1), pp. 5495-5504.
22. Rakshit, S., Agrawal, B. and Kumar, S. (2023), Scientific modelling of vascular blood circulation, *The Ciencia & Engenharia-Science & Engineering Journal*, vol. 11 (1), pp. 2908-2917.
23. Sahu, M.K., Sharma, S.K. and Agrawal A.K. (2010), Study of arterial blood flow in stenosed vessel using non-Newtonian couple stress fluid model, *International Journal of Dynamics of Fluids*, vol. 6(2) pp. 209-218.
24. Shah, S.R., Siddiqui, S.U. and Singh, A. (2016), Mathematical modeling and numerical simulation of blood flow through tapered artery, *International Journal of Innovative Science, Engineering & Technology*, vol. 3(2), pp. 710-717
25. Shukla, J. B., Parihar, R. S. and Gupta, S. P. (1980), Effects of peripheral layer viscosity on blood flow through the artery, *Bulletin of Mathematical Biology*, vol. 42(6), pp. 797-805.
26. Tantry, I.A., Wani, S. and Agrawal, B. (2021), Study of MHD boundary layer flow of a casson due to an exponentially stretching sheet with radiation effect, *Int. J. Stat. Appl. Math*, vol. 6(1), pp. 138-144.
27. Young, D. F. (1979), Fluid mechanics of arterial stenosis, *Journal of Biomechanical Engineering*, vol. 101(3), pp. 157-175.
28. Young, D.F. (1968), Effect of a time dependent stenosis on flow through a tube, *J. Engg. Ind. Trans. ASME*, vol. 90(5), pp. 248-254.